THE JOURNAL OF PHYSICAL CHEMISTRY Letters

Letter

pubs.acs.org/JPCL

Multiexciton Generation in IV–VI Nanocrystals: The Role of Carrier Effective Mass, Band Mixing, and Phonon Emission

Gal Zohar,[†] Roi Baer,*[,‡] and Eran Rabani*[,§]

[†]School of Physics and Astronomy, The Sackler Faculty of Sciences and [§]School of Chemistry, The Sackler Faculty of Exact Sciences, Tel Aviv University, Tel Aviv 69978, Israel

[‡]Fritz Haber Center for Molecular Dynamics, Institute of Chemistry, Hebrew University, Jerusalem 91904, Israel

ABSTRACT: We study the role of the effective mass, band mixing, and phonon emission on multiexciton generation in IV–VI nanocrystals. A four-band $k \cdot p$ effective mass model, which allows for an independent variation of these parameters, is adopted to describe the electronic structure of the nanocrystals. Multiexciton generation efficiencies are calculated using a Green's function formalism, providing results that are numerically similar to impact excitation. We find that multiexciton generation efficiencies are maximized when the effective mass of the electron and hole are small and similar. Contact with recent experimental results for multiexciton generation in PbS and PbSe is made.

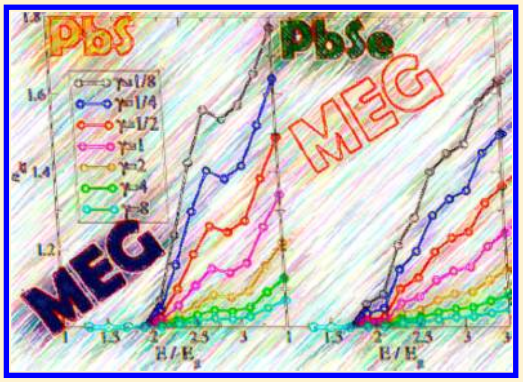

SECTION: Physical Processes in Nanomaterials and Nanostructures

The study of multiexciton generation (MEG) in nanocrystals (NCs) has received considerable attention in recent years, driving experiments[1−18] and theory.[14,19−35] While early stages have led to a controversy over efficiencies of MEG in confined systems, over the last several years, there is a consensus of efficiencies of 20−30% at $3E_g$(where E_g is the confined band gap),[23] depending on the size and composition of the NCs.

Despite advances made in the understanding of the MEG process, there are still many open questions. One of the most significant issues is related to the role of the effective mass of the carriers on the MEG efficiencies. On the one hand, the common wisdom suggests that a large ratio of effective masses should favor MEG because this would lead to asymmetric excitation where the lighter particle takes most of the excess photon energy, thereby reducing the threshold of MEG. On the other hand, materials such as PbS exhibit large MEG efficiencies, where the effective masses of the electron and hole are very similar.[3,18,36]

In this Letter, we address the role of the effective mass of the electron and hole on the MEG process. We resort to a four-band effective mass model,[37] which provides means to modify independently the effective mass of each charge carrier, preserving the remaining physical parameters. In addition, we explore the role of band mixing and the effect of the phonon emission rate on MEG efficiencies.

We follow the approach detailed in ref 26 to describe the MEG process. The electronic Hamiltonian can be partitioned as follows

$$H = H_0 + H_{ph} - \varepsilon\mu \sin(\omega t) \tag{1}$$

where H_0 is the unperturbed Hamiltonian of the various excitonic states and their Coulomb interactions

$$H_0 = \begin{pmatrix} E_0 & 0 & W_{0B} & \cdots \\ 0 & H_S & W_{SB} & \cdots \\ W_{0B}^{\dagger} & W_{SB}^{\dagger} & H_B & \cdots \\ \vdots & \vdots & \vdots & \ddots \end{pmatrix} \tag{2}$$

with E_0 the ground state energy of H_0. H_S and H_B are the Hamiltonian matrices of the single exciton subspace and biexciton subspace, respectively. Higher multiexciton states are ignored. We assume, as in Hartree−Fock theory, that the coupling of the ground state to any singly excited state vanishes, $W_{0S} = 0$ (Brillouin's theorem). As commonly assumed in solid-state theory, we neglect the contribution of higher excitons to the ground state, that is, $W_{0B} \approx 0$. W_{SB} describes the couplings between single excitons and biexcitons.[26]

$$W_{SB} = \delta_{ac}(V_{jikb} - V_{kijb}) + \delta_{ab}(V_{kijc} - V_{jikc}) + \delta_{ij}(V_{kcab} - V_{ackb}) + \delta_{ki}(V_{acjb} - V_{jcab}) \tag{3}$$

with the Coulomb matrix elements defined by

$$V_{rsut} = \frac{1}{\epsilon} \iint d^3r\, d^3r' \left[\frac{\psi_r^*(\mathbf{r})\psi_s(\mathbf{r})\psi_u^*(\mathbf{r}')\psi_t(\mathbf{r}')}{|\mathbf{r} - \mathbf{r}'|} \right] \tag{4}$$

Received: November 19, 2012
Accepted: December 31, 2012
Published: December 31, 2012

In the above equation, $\psi_r(\mathbf{r})$ are the single-particle spin orbitals and ϵ is the dielectric constant of the NC (assumed independent of $\mathbf{r}$ and $\mathbf{r}'$). We also do not assume spin degeneracy of the orbitals because, as discussed below, the wave functions for type IV−VI materials are not spin-degenerate.

In eq 1, H_{ph} represents the Hamiltonian of the phonons, but in the sequel, the electron−phonon interaction will be incorporated in a phenomenological way. The coupling to the electromagnetic field is described by the term $\varepsilon\mu \sin(\omega t)$, where

$$\mu = \begin{pmatrix} 0 & \mu_{0S} & 0 & \cdots \\ \mu_{0S}^{\dagger} & \mu_S & \mu_{SB} & \cdots \\ 0 & \mu_{SB}^{\dagger} & \mu_B & \cdots \\ \vdots & \vdots & \vdots & \ddots \end{pmatrix} \tag{5}$$

To obtain the MEG efficiency, we adopt the Green's function formalism discussed in ref 26 within the semi-wide-band limit. The rate for transition into single- and biexcitonic states following absorption of a photon of frequency ω is given by

$$r_S(\omega) = \frac{\varepsilon^2}{\hbar} \sum_S \frac{\gamma |\mu_{0S}|^2}{(E_0 + \hbar\omega - E_S)^2 + (\gamma + \Gamma_S)^2/4}$$

$$r_B(\omega) = \frac{\varepsilon^2}{\hbar} \sum_S \frac{\Gamma_S |\mu_{0S}|^2}{(E_0 + \hbar\omega - E_S)^2 + (\gamma + \Gamma_S)^2/4} \tag{6}$$

and the number of generated excitons is given by

$$n_{ex}(\omega) = \frac{\sum_S \frac{(\hbar\gamma + 2\hbar\Gamma_S)|\mu_S|^2}{(E_0 + \hbar\omega - E_S)^2 + (\hbar\gamma + \hbar\Gamma_S)^2/4}}{\sum_S \frac{(\hbar\gamma + \hbar\Gamma_S)|\mu_S|^2}{(E_0 + \hbar\omega - E_S)^2 + (\hbar\gamma + \hbar\Gamma_S)^2/4}} \tag{7}$$

where γ is the phonon decay rate, assumed to be independent of the energy, $\Gamma_S = (2\pi/\hbar)\sum_B |W_{SB}|^2 \delta(E - E)$ is the rate of the decay of a single exciton $|S\rangle$ to biexcitons,[26] and E_0, E_S, and E_B are the ground-state and singly and doubly excited-state energies, respectively. μ_S is the transition dipole between the ground state and the singly excited state $|S\rangle$, where the hole (electron) is in state $|\psi_i\rangle$ ($|\psi_a\rangle$)

$$|\mu_S|^2 = \frac{1}{3}\sum_i |\langle\psi_a|\mathbf{e}_i\cdot\mathbf{p}|\psi_i\rangle|^2 \tag{8}$$

Here, $\mathbf{e}_i$ is the unit vector representing the direction of light polarization and $\mathbf{p} = -i\hbar\nabla$ is the momentum operator.

We adopt a four-band effective mass model developed by Kang and Wise[37] for calculating eigenstates and eigenenergies for the IV−VI NCs. While the approach does not account for the asymmetry in the hole density of states predicted by atomistic calculations,[19,38] it provides simple means to change the relevant parameters and study how this affects MEG. The Hamiltonian in the spherical approximations is given by

$$H_0(\mathbf{k}) = \begin{pmatrix} \left(\frac{E_g^{bulk}}{2} + \frac{\hbar^2k^2}{2m_e}\right)\mathbf{1} & \frac{\hbar P}{m_0}\mathbf{k}\cdot\boldsymbol{\sigma} \\ \frac{\hbar P}{m_0}\mathbf{k}\cdot\boldsymbol{\sigma} & -\left(\frac{E_g^{bulk}}{2} + \frac{\hbar^2k^2}{2m_h}\right)\mathbf{1} \end{pmatrix} \tag{9}$$

where E_g^{bulk} is the bulk band gap, P is the coupling parameter between the valence and conduction bands, m_0 is the electron mass, m_h and m_e are the effective masses of the hole and electron, respectively, and $\boldsymbol{\sigma}$ are Pauli matrices.

The spin orbital is represented as a sum over each element of the vector wave function multiplied by the appropriate band edge Bloch function $u_s(\mathbf{r})$

$$\psi_i(\mathbf{r}) = \sum_{s=1}^{4} \phi_s^i(\mathbf{r}) u_s(\mathbf{r}) \tag{10}$$

where $i \equiv (n,m,j,\pi)$ is a composite index depending on the parity and angular momentum of the state. The boundary conditions $\phi_s^i(R) = 0$, where R is the radii of the NCs, are imposed, corresponding to approximating the confinement potential as an infinite step function. The above model Hamiltonian has an exact solution given by[37]

$$\phi^{(n,j,m,(-1)^{l+1})} = \frac{N_{n,j,m,(-1)^{l+1}}}{R^{3/2}} \begin{pmatrix} i\left[j_l(k_\pm r) + \frac{j_l(k_\pm R)}{i_l(\lambda_\pm(k)R)} i_l(\lambda_\pm(k) r)\right] \begin{pmatrix} \sqrt{\frac{l+m+\frac{1}{2}}{2l+1}}\, Y_{l,m-1/2}(\theta,\varphi) \\ -\sqrt{\frac{l-m+\frac{1}{2}}{2l+1}}\, Y_{l,m+1/2}(\theta,\varphi) \end{pmatrix} \\ -\rho_\pm(k_\pm)\left[j_{l+1}(k_\pm r) + \frac{j_{l+1}(k_\pm R)}{i_{l+1}(\lambda_\pm(k)R)} i_{l+1}(\lambda_\pm(k) r)\right] \begin{pmatrix} \sqrt{\frac{l-m+\frac{3}{2}}{2l+1}}\, Y_{l+1,m-1/2}(\theta,\varphi) \\ \sqrt{\frac{l+m+\frac{3}{2}}{2l+3}}\, Y_{l+1,m+1/2}(\theta,\varphi) \end{pmatrix} \end{pmatrix} \tag{11}$$

dx.doi.org/10.1021/jz301892z | J. Phys. Chem. Lett. 2013, 4, 317−322

and

$$\phi^{(n,j,m,(-1)^l)} = \frac{N_{n,j,m,(-1)^l}}{R^{3/2}} \begin{pmatrix} i\left[j_{l+1}(k_\pm r) + \frac{j_{l+1}(k_\pm R)}{i_{l+1}(\lambda_\pm(k)R)} i_{l+1}(\lambda_\pm(k) r)\right] \begin{pmatrix} \sqrt{\frac{l-m+\frac{3}{2}}{2l+1}}\, Y_{l+1,m-1/2}(\theta,\varphi) \\ -\sqrt{\frac{l+m+\frac{3}{2}}{2l+3}}\, Y_{l+1,m+1/2}(\theta,\varphi) \end{pmatrix} \\ -\rho_\pm(k_\pm)\left[j_l(k_\pm r) + \frac{j_l(k_\pm R)}{i_l(\lambda_\pm(k)R)} i_l(\lambda_\pm(k) r)\right] \begin{pmatrix} \sqrt{\frac{l+m+\frac{1}{2}}{2l+1}}\, Y_{l,m-1/2}(\theta,\varphi) \\ \sqrt{\frac{l-m+\frac{1}{2}}{2l+1}}\, Y_{l,m+1/2}(\theta,\varphi) \end{pmatrix} \end{pmatrix} \tag{12}$$

with eigenenergies of the electrons (+) and holes (−) given by

$$E_\pm(k) = \frac{1}{2}\left[\gamma k^2 \pm \sqrt{(E_g^{bulk} + \alpha k^2)^2 + \beta^2 k^2}\right] \tag{13}$$

where

$$\lambda_\pm(k) = \sqrt{\frac{2\alpha E_g^{bulk} + \beta^2 + (\alpha^2 - \gamma^2)k^2 + 4\gamma E_\pm(k)}{\alpha^2 - \gamma^2}} \tag{14}$$

In the above equations, $\alpha = \hbar^2/2m_h + \hbar^2/2m_e$, $\beta = 2\hbar P/m_0$, $\gamma = \hbar^2/2m_h - \hbar^2/2m_e$. $j_l(x)$ and $i_l(x)$ are the spherical Bessel and modified spherical Bessel functions of the first kind, respectively, and $Y_{l,m}(\theta,\varphi)$ are the spherical harmonics.[39] The quantum numbers $n = [1, 2, ...]$, $j = l + 1/2$ ($l = 0, 1, ...$), $m = [-j,..., j]$, and $\pi = \pm 1$ correspond to the energy level, total angular momentum, projection of the angular momentum, and parity, respectively. The value of k is given by the nth lowest positive solution of the equations

$$\rho_\pm(k) j_{l+1}(ka) i_l(\lambda_\pm a) - \mu_\pm(k) j_l(ka) i_{l+1}(\lambda_\pm a) = 0 \tag{15}$$

for $\pi = (-1)^l$ or

$$\rho_\pm(k) j_l(ka) i_{l+1}(\lambda_\pm a) + \mu_\pm(k) j_{l+1}(ka) i_l(\lambda_\pm a) = 0 \tag{16}$$

for $\pi = (-1)^{l+1}$, and $\rho_\pm(k)$ and $\mu_\pm(k)$ are defined as

$$\rho_\pm(k) = \frac{1}{\beta k}\left[\frac{E_g}{2} + (\alpha + \gamma)k^2 - 2E_\pm(k)\right]$$
$$\mu_\pm(k) = \frac{1}{\beta \lambda_\pm(k)}\left[E_g - (\alpha + \gamma)\lambda_\pm(k)^2 - 2E_\pm(k)\right] \tag{17}$$

The normalization is given by

$$\frac{1}{N_{n,j,m,(-1)^{l+1}}^2} = \int_{x=0}^{1} x^2\, dx \times \left(\left\{\rho_\pm(k_\pm)\left[j_{l+1}(k_\pm Rx) + \frac{j_{l+1}(k_\pm R)}{i_{l+1}(\lambda_\pm(k)R)} i_{l+1}(\lambda_\pm(k)Rx)\right]\right\}^2 + \left[j_l(k_\pm Rx) + \frac{j_l(k_\pm R)}{i_l(\lambda_\pm(k)R)} i_l(\lambda_\pm(k)Rx)\right]^2\right)$$
$$\frac{1}{N_{n,j,m,(-1)^l}^2} = \int_{x=0}^{1} x^2\, dx \times \left(\left\{\rho_\pm(k_\pm)\left[j_l(k_\pm ax) + \frac{j_l(k_\pm a)}{i_l(\lambda_\pm(k)a)} i_l(\lambda_\pm(k)ax)\right]\right\}^2 + \left[j_{l+1}(k_\pm ax) + \frac{j_{l+1}(k_\pm a)}{i_{l+1}(\lambda_\pm(k)a)} i_{l+1}(\lambda_\pm(k)ax)\right]^2\right) \tag{18}$$

The above wave functions and energies are then used to evaluate numerically the matrix elements of V_{rsut} given by eq 4, the rate Γ_S, and the number of excitons generated upon excitation (cf., eq 7). In Table 1, we provide the values for the model parameters for PbS and PbSe.

Table 1. Four-Band Effective Mass Model Parameters from PbS and PbSe

	E_g^{bulk} (eV)	m_0/m_e	m_0/m_h	$2P^2/m_0$ (eV)	ϵ
PbS	0.41	2.5	3.0	2.5	17
PbSe	0.28	3.9	6.9	2.6	23

To quantify the role of the effective masses of the charge carriers on the efficiency of MEG, we have preformed a set of calculations for two electron effective masses, $m_e/m_0 = 1/6$ and 2, and for a range of hole effective masses, $m_h/m_0 = 1/6$, 2/5, 2/3, and 2. Other model parameters are based on the PbS parameters of Table 1. The phonon decay rate was taken as $\gamma = 1\ ps^{-1}$. The results for a QD of 10 nm diameter are shown in Figure 1, where we plot the average number of excitons generated as a function of the excitation energy (in scaled units E/E_g, where E_g is the fundamental gap of the NC) for different effective masses. Left and right panels display the results for a light and heavy electron, respectively. The results are averaged over a 5% size distribution of the NCs and an energy window of $\sim\pm 1/4E_g$.

dx.doi.org/10.1021/jz301892z | J. Phys. Chem. Lett. 2013, 4, 317−322

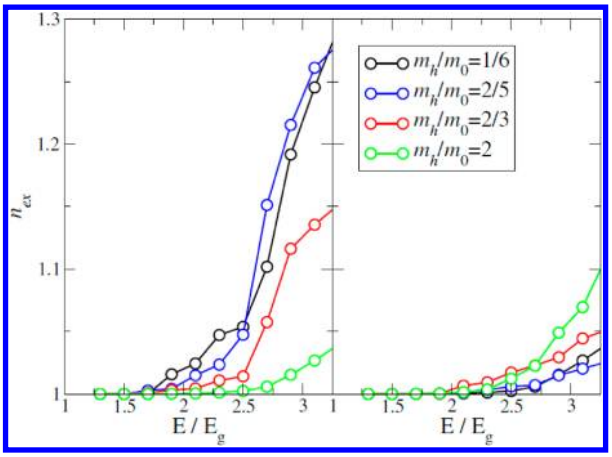

Figure 1. Number of excitons per photon, n_{ex}, as a function of scaled energy (E/E_g) for various values of the hole effective masses. The left panel shows the results for an electron effective mass of m_e/m_0 = 1/6, and the right panel shows results for an electron effective mass of m_e/m_0 = 2. The remaining parameters are for a PbS NC with a diameter of 10 ± 0.5 nm. The results are averaged over an energy window of $\pm 1/4E_g$.

The general trends and the conclusions that can be drawn are quite clear. We find that when the effective masses of the two carriers are quite similar, MEG efficiencies are larger compared to the case where the two masses differ significantly, at the energy range shown. Moreover, the onset of MEG is below $3E_g$ even when the two masses are equal as a result of band mixing. Highest MEG efficiencies occur when the effective masses of both carriers are small and similar. Because the results are based on Fermi's golden rule, which breaks down for very small effective masses due to the decrease in the density of states, there is a lower bound on the magnitude of the effective mass that can be calculated with the current approach. The behavior seen in Figure 1 holds qualitatively for different phonon emission rates or for other NC sizes, varied within an experimentally relevant range.

In Figure 2, we plot the average value of the Coulomb couplings, $\langle W_a \rangle = [(\hbar/2\pi)\Gamma_a^-/\rho_T^-]^{1/2}$, for the electron decay,

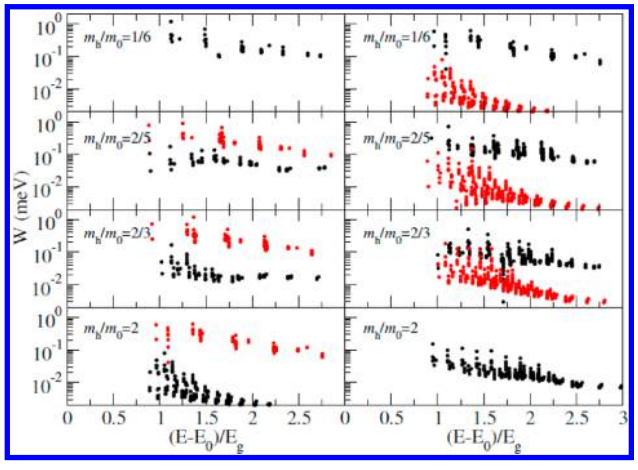

Figure 2. The average Coulomb coupling for electrons (red symbols) and holes (black symbols) for a 10 nm diameter NC as a function of the scaled energy. The different panels represent different values of the hole effective mass. Left and right panels are for m_e/m_0 = 1/6 and 2, respectively.

where Γ_a^- is the negative trion formation rate and ρ_T^- is the corresponding density of trion states (DOTS).[35] A similar expression, with $a \rightarrow i$ and $- \rightarrow +$, holds for the holes. Red and black symbols correspond to the average value $\langle W \rangle$ for electrons and holes in a given initial state, respectively. We first analyze the case when the effective mass of the electron equals that of the hole (upper left and lower right panels of Figure 2). Due to the symmetric band structure assumed by the model, the results for electrons and holes coincide in each case separately. At a given energy, $\langle W \rangle$ increases as the effective mass decreases because the corresponding wave functions are less oscillatory giving rise to larger two-electron integrals. This is evident comparing the results for $m_e/m_0 = m_h/m_0 = 2$ and 1/6. In the calculation of MEG efficiencies, the larger value of $\langle W \rangle$ for smaller masses overtakes the decrease in the DOTS (not shown here), leading to an overall increase of MEG efficiencies for small effective mass (see Figure 1).

When the two masses differ, $\langle W \rangle$ shows two distinct regimes with a *smaller* value for the *heavier* particle. In this case, the lighter particle can take most of the excitation energy and also, as explained above, assumes a larger value for $\langle W \rangle$ (see, for example, the lower left panel in Figure 2). Comparing the trion formation rates of the lighter particle, we find that they are only slightly influenced by an increase of the mass of the heavier particle. This, apparently, suggests that MEG would favor a large ratio of the effective masses, in contrast to the results shown in Figure 1.

This apparent paradox can be rationalized as follows. It turns out that the intuitive assumption that the lighter particle takes most of the excitation energy is, in fact, incorrect. Indeed, transitions where the lighter particle takes the excess energy are much stronger than other transitions. However, the density of singly excited states, where the heavy particle takes the excess energy, is much larger. Thus, the effective oscillator strength of such transitions is larger, often by 2 orders of magnitude. Because the average Coulomb coupling of the heavier particle is significantly lower, the overall efficiency decreases when the two masses differ, consistent with the results shown in Figure 1.

In order to test the effects of the coupling strength between the conduction and valence bands on MEG,[29,40,41] we have repeated the calculations by artificially changing the value of P in the Hamiltonian given by eq 9. In Figure 3, we plot the MEG

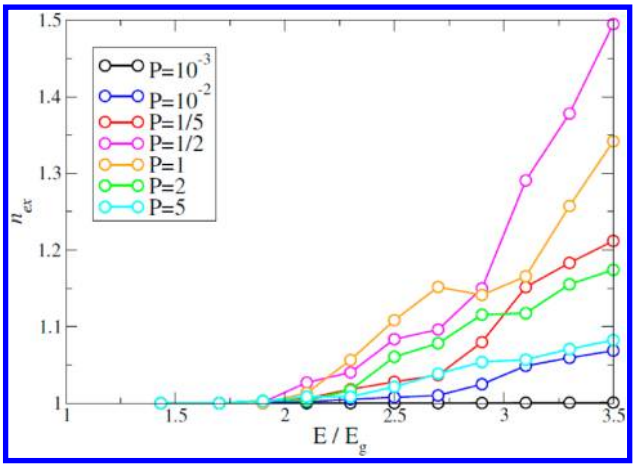

Figure 3. Number of excitons per photon, n_{ex}, as a function of scaled energy for various values of the band coupling strength, P (relative to the value of P for PbS). The remaining parameters are taken for a 10 nm diameter PbS NC. The results are averaged over an energy window of $\pm 1/4E_g$.

efficiencies for different values of P. MEG efficiencies vanish with diminishing band couplings, consistent with the fact that for a

dx.doi.org/10.1021/jz301892z | J. Phys. Chem. Lett. 2013, 4, 317−322

two-band model ($P \rightarrow 0$), the Coulomb coupling elements, V_{rsut}, are zero. When P is very large, the confinement energies increase relative to the bulk band gap, and thus, the density of states decreases, leading to very small MEG efficiencies. At intermediate values of P, MEG assumes a maximal efficiency. For the present case, this occurs for values that are close to those of PbS.

The density of trion states increases rapidly with increasing excitation energies, leading to a rapid increase in the MEG rates. Thus, one would expect that different phonon emission rates will only shift the onset of MEG. If, however, the increase of MEG rates near values comparable to the phonon emission rate is rather slow, then the changes in the phonon emission rate may significantly affect the efficiency of MEG.

In Figure 4, we plot the efficiency of MEG for various values of the phonon emission rates for PbS and PbSe NCs with a

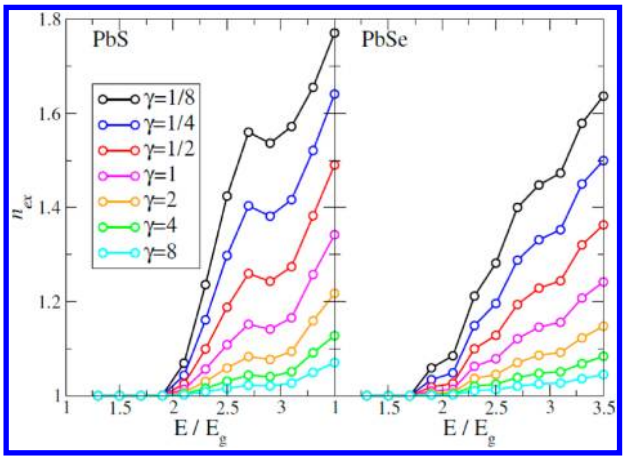

Figure 4. Number of excitons per photon, n_{ex}, as a function of the scaled energy for various phonon emission rates, calculated for 10 nm diameter PbS (left) and PbSe (right) NCs. The results are averaged over an energy window of $\pm 1/4E_g$.

diameter of 10 nm. The change in the phonon emission rate does not shift the onset of MEG but rather changes the overall MEG efficiency. Even when the phonon emission rate increases by just a factor of 2, it leads to a decrease of the MEG efficiency by a similar factor. Comparing the results for PbS and PbSe, it is clear that differences observed in the MEG efficiencies result from the differences in the phonon emission rate and not from the differences in effective masses and band gaps, consistent with recent experimental reports.[16,18]

We note in passing that in the calculations reported here, we assumed that the phonon emission rate is energy-independent. Thus, our MEG yields may be considered as upper bound because we expect the phonon emission rate to increase with energy.[42,43] The exact energy dependence of the phonon emission rate is a topic of research in its own right and will be discussed in future studies.

In this Letter, we addressed the role of the effective mass of the electron and hole on MEG. We showed that when the two masses are equal and small, MEG efficiencies were maximized, consistent with high MEG efficiencies reported for PbS. This is a result of the rapid increase in the Coulomb coupling relative to the slower decrease in the DOTS when the effective mass is reduced. Moreover, when the effective mass of the electron and hole are significantly different, as a result of asymmetric excitations allowed by band mixing, the MEG efficiencies are reduce because excess energy given to the heavier particle does not contribute to the formation of multiexcitons.

We have also studied the role of couplings between the bands and the impact of the phonon emission rate on MEG. The former shows a maximum value for MEG efficiencies near coupling values of PbS. Variations in the phonon emission rate lead to an overall change in the MEG efficiencies, rather than shifting the onset of MEG. The differences observed experimentally between PbS and PbSe can be attributed to the difference in the phonon emission rate. For equal phonon emission rates, the two show similar MEG efficiencies, despite having different electron and hole model parameters.

AUTHOR INFORMATION

Corresponding Author

*E-mail: roi.baer@gmail.com (R.B.); eran.rabani@gmail.com (E.R.).

Notes

The authors declare no competing financial interest.

ACKNOWLEDGMENTS

This research was supported by the Israel Science Foundation (Grant Numbers 611/11, 1020/10) and by the FP7Marie Curie IOF project HJSC. E.R. would like to thank the Center for Re-Defining Photovoltaic Efficiency Through Molecule Scale Control, an Energy Frontier Research Center funded by the U.S. Department of Energy, Office of Science, Office of Basic Energy Sciences under Award Number DE-SC0001085.

REFERENCES

(1) Schaller, R. D.; Klimov, V. I. High Efficiency Carrier Multiplication in PbSe Nanocrystals: Implications for Solar Energy Conversion. *Phys. Rev. Lett.* **2004**, *92*, 186601.

(2) Schaller, R. D.; Petruska, M. A.; Klimov, V. I. Effect of Electronic Structure on Carrier Multiplication Efficiency: Comparative Study of PbSe and CdSe Nanocrystals. *Appl. Phys. Lett.* **2005**, *87*, 253102.

(3) Ellingson, R. J.; Beard, M. C.; Johnson, J. C.; Yu, P. R.; Micic, O. I.; Nozik, A. J.; Shabaev, A.; Efros, A. L. Highly Efficient Multiple Exciton Generation in Colloidal PbSe and PbS Quantum Dots. *Nano Lett.* **2005**, *5*, 865−871.

(4) Schaller, R. D.; Agranovich, V. M.; Klimov, V. I. High-Efficiency Carrier Multiplication through Direct Photogeneration of Multi-Excitons via Virtual Single-Exciton States. *Nat. Phys.* **2005**, *1*, 189−194.

(5) Klimov, V. I. Mechanisms for Photogeneration and Recombination of Multiexcitons in Semiconductor Nanocrystals: Implications for Lasing and Solar Energy Conversion. *J. Phys. Chem. B* **2006**, *110*, 16827−16845.

(6) Schaller, R. D.; Sykora, M.; Pietryga, J. M.; Klimov, V. I. Seven Excitons at a Cost of One: Redefining the Limits for Conversion Efficiency of Photons into Charge Carriers. *Nano Lett.* **2006**, *6*, 424−429.

(7) Murphy, J. E.; Beard, M. C.; Norman, A. G.; Ahrenkiel, S. P.; Johnson, J. C.; Yu, P. R.; Micic, O. I.; Ellingson, R. J.; Nozik, A. J. PbTe Colloidal Nanocrystals: Synthesis, Characterization, And Multiple Exciton Generation. *J. Am. Chem. Soc.* **2006**, *128*, 3241−3247.

(8) Pijpers, J. J. H.; Hendry, E.; Milder, M. T. W.; Fanciulli, R.; Savolainen, J.; Herek, J. L.; Vanmaekelbergh, D.; Ruhman, S.; Mocatta, D.; Oron, D.; et al. Carrier Multiplication and Its Reduction by Photodoping in Colloidal InAs Quantum Dots. *J. Phys. Chem. C* **2007**, *111*, 4146−4152.

(9) Schaller, R. D.; Pietryga, J. M.; Klimov, V. I. Carrier Multiplication in InAs Nanocrystal Quantum Dots with an Onset Defined by the Energy Conservation Limit. *Nano Lett.* **2007**, *7*, 3469−3476.

(10) Beard, M. C.; Knutsen, K. P.; Yu, P. R.; Luther, J. M.; Song, Q.; Metzger, W. K.; Ellingson, R. J.; Nozik, A. J. Multiple Exciton Generation in Colloidal Silicon Nanocrystals. *Nano Lett.* **2007**, *7*, 2506−2512.
(11) Nair, G.; Bawendi, M. G. Carrier Multiplication Yields of CdSe and CdTe Nanocrystals by Transient Photoluminescence Spectroscopy. *Phys. Rev. B* **2007**, *76*, 081304.
(12) Ben-Lulu, M.; Mocatta, D.; Bonn, M.; Banin, U.; Ruhman, S. On the Absence of Detectable Carrier Multiplication in a Transient Absorption Study of InAs/CdSe/ZnSe Core/Shell1/Shell2 Quantum Dots. *Nano Lett.* **2008**, *8*, 1207−1211.
(13) Nair, G.; Geyer, S. M.; Chang, L. Y.; Bawendi, M. G. Carrier Multiplication Yields in PbS and PbSe Nanocrystals Measured by Transient Photoluminescence. *Phys. Rev. B* **2008**, *78*, 125325.
(14) Pijpers, J. J. H.; Ulbricht, R.; Tielrooij, K. J.; Osherov, A.; Golan, Y.; Delerue, C.; Allan, G.; Bonn, M. Assessment of Carrier-Multiplication Efficiency in Bulk PbSe and PbS. *Nat.Phys.* **2009**, *5*, 811−814.
(15) McGuire, J. A.; Sykora, M.; Joo, J.; Pietryga, J. M.; Klimov, V. I. Apparent Versus True Carrier Multiplication Yields in Semiconductor Nanocrystals. *Nano Lett.* **2010**, *10*, 2049−2057.
(16) Nair, G.; Chang, L. Y.; Geyer, S. M.; Bawendi, M. G. Perspective on the Prospects of a Carrier Multiplication Nanocrystal Solar Cell. *Nano Lett.* **2011**, *11*, 2145−2151.
(17) Gdor, I.; Sachs, H.; Roitblat, A.; Strasfeld, D. B.; Bawendi, M. G.; Ruhman, S. Exploring Exciton Relaxation and Multiexciton Generation in PbSe Nanocrystals Using Hyperspectral Near-IR Probing. *ACS Nano* **2012**, *6*, 3269−3277.
(18) Stewart, J. T.; Padilha, L. A.; Qazilbash, M. M.; Pietryga, J. M.; Midgett, A. G.; Luther, J. M.; Beard, M. C.; Nozik, A. J.; Klimov, V. I. Comparison of Carrier Multiplication Yields in PbS and PbSe Nanocrystals: The Role of Competing Energy-Loss Processes. *Nano Lett.* **2012**, *12*, 622−628.
(19) Franceschetti, A.; An, J. M.; Zunger, A. Impact Ionization Can Explain Carrier Multiplication in PbSe Quantum Dots. *Nano Lett.* **2006**, *6*, 2191−2195.
(20) Shabaev, A.; Efros, A. L.; Nozik, A. J. Multiexciton Generation by a Single Photon in Nanocrystals. *Nano Lett.* **2006**, *6*, 2856−2863.
(21) Allan, G.; Delerue, C. Role of Impact Ionization in Multiple Exciton Generation in PbSe Nnocrystals. *Phys. Rev. B* **2006**, *73*, 205423.
(22) Califano, M.; Franceschetti, A.; Zunger, A. Lifetime and Polarization of the Radiative Decay of Excitons, Biexcitons, And Trions in CdSe Nanocrystal Quantum Dots. *Phys. Rev. B* **2007**, *75*, 115401.
(23) Rabani, E.; Baer, R. Distribution of Multiexciton Generation Rates in CdSe and InAs Nanocrystals. *Nano Lett.* **2008**, *8*, 4488−4492.
(24) Isborn, C. M.; Kilina, S. V.; Li, X. S.; Prezhdo, O. V. Generation of Multiple Excitons in PbSe and CdSe Quantum Dots by Direct Photoexcitation: First-Principles Calculations on Small PbSe and CdSe Clusters. *J. Phys. Chem. C* **2008**, *112*, 18291−18294.
(25) Isborn, C. M.; Prezhdo, O. V. Charging Quenches Multiple Exciton Generation in Semiconductor Nanocrystals: First-Principles Calculations on Small PbSe Clusterse. *J. Phys. Chem. C* **2009**, *113*, 12617−12621.
(26) Rabani, E.; Baer, R. Theory of Multiexciton Generation in Semiconductor Nanocrystals. *Chem. Phys. Lett.* **2010**, *496*, 227−235.
(27) Baer, R.; Rabani, E. Can Impact Excitation Explain Efficient Carrier Multiplication in Carbon Nanotube Photodiodes? *Nano Lett.* **2010**, *10*, 3277−3282.
(28) Witzel, W. M.; Shabaev, A.; Hellberg, C. S.; Jacobs, V. L.; Efros, A. L. Quantum Simulation of Multiple-Exciton Generation in a Nanocrystal by a Single Photon. *Phys. Rev. Lett.* **2010**, *105*, 137401.
(29) Striolo, A.; Ward, J.; Prausnitz, J. M.; Parak, W. J.; Zanchet, D.; Gerion, D.; Milliron, D.; Alivisatos, A. P. Molecular Weight, Osmotic Second Virial Coefficient, and Extinction Coefficient of Colloidal CdSe Nanocrystals. *J. Phys. Chem. B* **2002**, *106*, 5500−5505.
(30) Delerue, C.; Allan, G.; Pijpers, J. J. H.; Bonn, M. Carrier Multiplication in Bulk and Nanocrystalline Semiconductors: Mechanism, Efficiency, And Interest for Solar Cells. *Phys. Rev. B* **2010**, *81*, 125306.
(31) Lin, Z. B.; Franceschetti, A.; Lusk, M. T. Size Dependence of the Multiple Exciton Generation Rate in CdSe Quantum Dots. *ACS Nano* **2011**, *5*, 2503−2511.
(32) Allan, G.; Delerue, C. Optimization of Carrier Multiplication for More Effcient Solar Cells: The Case of Sn Quantum Dots. *Acs Nano* **2011**, *5*, 7318−7323.
(33) Velizhanin, K. A.; Piryatinski, A. Numerical Study of Carrier Multiplication Pathways in Photoexcited Nanocrystal and Bulk Forms of PbSe. *Phys. Rev. Lett.* **2011**, *106*, 207401.
(34) Velizhanin, K. A.; Piryatinski, A. Numerical Analysis of Carrier Multiplication Mechanisms in Nanocrystalline and Bulk Forms of PbSe and PbS. *Phys. Rev. B* **2012**, *86*, 165319.
(35) Baer, R.; Rabani, E. Expeditious Stochastic Calculation of Multiexciton Generation Rates in Semiconductor Nanocrystals. *Nano Lett.* **2012**, *12*, 2123−2128.
(36) Trinh, M. T.; Polak, L.; Schins, J. M.; Houtepen, A. J.; Vaxenburg, R.; Maikov, G. I.; Grinbom, G.; Midgett, A. G.; Luther, J. M.; Beard, M. C.; et al. Anomalous Independence of Multiple Exciton Generation on Different Group IV−I Quantum Dot Architectures. *Nano Lett.* **2011**, *11*, 1623−1629.
(37) Kang, I.; Wise, F. W. Electronic Structure and Optical Properties of PbS and PbSe Quantum Dots. *J. Opt. Soc. Am. B* **1997**, *14*, 1632−1646.
(38) Wang, L. W.; Zunger, A. Local-Density-Derived Semiempirical Pseudopotentials. *Phys. Rev. B* **1995**, *51*, 17398−17416.
(39) Abramowitz, M.; Stegun, I. A. *Handbook of Mathematical Functions with Formulas, Graphs, and Mathematical Tables*, 10th ed.; U.S. Department of Commerce: Washington, DC, 1972; Vol. *55*.
(40) Jones, R. O.; Gunnarsson, O. The Density Functional Formalism, Its Applications and Prospects. *Rev. Mod. Phys.* **1989**, *61*, 689−746.
(41) Roy, D.; Marianski, M.; Maitra, N. T.; Dannenberg, J. J. Comparison of Some Dispersion-Corrected and Traditional Functionals with CCSD(T) and MP2 Ab Initio Methods: Dispersion, Induction, And Basis Set Superposition Error. *J. Chem. Phys.* **2012**, *137*, 134109−134112.
(42) Cooney, R. R.; Sewall, S. L.; Anderson, K. E. H.; Dias, E. A.; Kambhampati, P. Breaking the Phonon Bottleneck for Holes in Semiconductor Quantum Dots. *Phys. Rev. Lett.* **2007**, *98*, 177403.
(43) Cohen, M.; Chelikowsky, J. *Electronic Structure and Optical Properties of Semiconductors*; Springer Verlag: Berlin, Germany, 1988.